Journal of Alloys and Metallurgical Systems 5 (2024) 100062

Contents lists available at ScienceDirect

Journal of Alloys and Metallurgical Systems

journal homepage: www.journals.elsevier.com/journal-of-alloys-and-metallurgical-systems

Solute Effects on Growth Restriction in Dilute Ferrous Alloys

María J. Balart [a,*,1], Fabio Miani [b]

[a] University of Warwick, WMG – Energy Innovation Centre (EIC), Coventry CV4 7AL, UK
[b] Dipartimento Politecnico di Ingegneria e Architettura (DPIA), University of Udine, Via delle Scienze 208, Udine 33100 , Italy

ARTICLE INFO

Keywords:
Grain size
Solidification
Growth restriction parameter
Grain refinement
Dilute
Ferrous alloys

ABSTRACT

The effect of dilute solute additions on growth restriction in binary ferrous alloys has been assessed by means of the heuristic growth restriction parameter (β) modelling framework (Fan *et al.* in Acta Mater. 152, 248–257, 2018). The CALPHAD (CALculation of PHAse Diagrams) methodology (Kaufman and Bernstein in Computer Calculation of Phase Diagrams, 1970) has been used to calculate β values from the liquidus slope m and the equilibrium distribution coefficient k values, at first approximation, in conjunction with the liquid-to-solid fraction to obtain *true* β values. Critical solute concentrations, below which solidification becomes partitionless, have also been calculated. Among 23 dilute binary ferrous alloy systems investigated, the five most efficient solutes on grain refinement are B, Y, O, S and C. A negative correlation, or inverse relationship, was observed between the *true* β values and the grain size values obtained from a study on experimental multicomponent dilute ferrous alloy systems (Li *et al.* in Metall. Mater. Trans. A 49 A, 2235–2247, 2018).

1. Introduction

Dilute ferrous alloys are increasingly in demand in the energy and transportation sectors for electrical steels [1,2] and some low-density ferritic steel grades [3,4] applications, for example, electrical motors, transformers, and vehicle structure. Binary alloys are typically categorized as dilute binary alloys if solute additions are made below a threshold of 10 at pct [5], or otherwise, are concentrated binary alloys. Their electrical and mechanical properties are critically dependent on the grain size. In addition, some dilute binary FeGd alloy grades could have a potential application for spent nuclear fuel (SNF) [6].

The final performance–i.e. strength, toughness, reliability, lifetime, etc– of the products in the as-cast condition and after the application of deformation and subsequent heat-treatments, is controlled by the microstructure of the castings during solidification. Casting defects–e.g., porosity, hot tears, shrinkage and segregation– contribute to reduced mechanical properties. Very limited data of grain size analysis in steels in the as-cast condition are available [7]. Li *et al.* [7] investigated the effects of increased amounts of solute additions of B, Zr, Y, Cu and Mo on the as-cast grain structure of experimental Fe-4Si ferritic alloys at a constant superheat of 80 K. Fe-4Si ferritic alloy was purposely designed to maintain a whole δ-ferrite microstructure during solidification without subsequent phase transformations in the solid state. Y is an uncommon alloying element in steels.

Fan *et al.* [8] have introduced a new concept for growth restriction during solidification. This pioneering research produced several innovative findings, some of which are highlighted here. Moreover, Fan et al. [9] recently published a thorough review and overview of the impact of solutes on grain refining, helping to identify near-future challenges.

The heuristic growth restriction parameter (β) was formulated by Fan *et al.* [8] to account for the effects of the liquidus slope (m), solute concentration (C_O), equilibrium distribution coefficient (k) and a fixed undercooling during solidification (ΔT) on the growth restriction of equiaxed grains as follows:

$$\beta = \frac{mC_O(k-1)}{\Delta T} - k = \frac{Q}{\Delta T} - k \quad (1)$$

where the *conventional* growth restriction factor Q is:

$$Q = mC_O(k-1) \quad (2)$$

The heuristic solution for the accurate calculation of *true* β values was obtained by replacing $\Delta T = m(C_O - C_L)$ and $k = C_S / C_L$ into Eq. 1 for a binary system (Eq. 3), which could be extended to multicomponent systems by linear addition of each binary system β_i (Eq. 4) [8].

* Corresponding author.
E-mail address: Maria.Balart-Murria@warwick.ac.uk (M.J. Balart).
[1] Previous address: Brunel Centre for Advanced Solidification Technology (BCAST), Brunel University London, Uxbridge, UB8 3PH, UK

https://doi.org/10.1016/j.jalmes.2024.100062
Received 29 November 2023; Received in revised form 8 February 2024; Accepted 12 February 2024
Available online 13 February 2024

Table I
m, *k*, *C** and CoV of *k* values for the dilute binary ferrous alloys investigated.

Solute	*m*	*k*	*C**	Wt pct (10 at pct)	CoV of *k* (pct)
Al	-2.67	0.954	3.87	5.09	0 (8.26)
B	-83.81	0.0006	0.000004	1.92	14.96
C	-82.00	0.177	0.001	2.33	0.24
Ca	-5.98	0.782	0.30	15.22	0.18
Ce	-6.94	0.019	0.0014	21.80	21.01
Co	-1.19 → −1.513 → -1.76 → −2.06	0.944 → 0.923 → 0.917 → 0.912	7.15 → 3.96 → 3.16 → 2.51	10.49	0.98
Cr	-1.50	0.939	5.17	9.38	0.93
Cu	-3.39	0.681	0.32	11.22	10.46
Mg	-24.12	0.422	0.015	4.61	2.30
Mn	-5.07	0.761	0.31	9.85	1.16
Mo	-2.45	0.820	0.93	16.03	1.13
Nb	-10.25	0.255	0.017	15.60	9.44
Ni	-3.87	0.793	0.49	10.46	1.03
O	-61.66	0.060	0.0005	3.09	2.66
P	-25.82	0.237	0.006	5.80	4.85
S	-31.37	0.042	0.0007	6.00	5.14 (29.36)
Si	-10.94 → −12.77 → −15.23 → −17.08 → −18.88 → −20.14	0.732→ 0.707 → 0.707 → 0.718 → 0.737 → 0.756	0.125 → 0.094 → 0.079 → 0.075 → 0.074 → 0.077	5.29	2.38
Ti	-15.94	0.346	0.017	8.70	7.15 (18.13)
V	-3.34	0.862	0.94	9.14	1.70
W	0.57 → 0.81 → 1.04 → 1.33	1.055 → 1.068 → 1.082 → 1.102	16.92 → 9.74 → 6.29 → 4.06	26.78	1.64 (6.77)
Y	-13.87	0.0002	0.000007	15.03	11.26
Zn	-5.07	0.684	0.21	11.51	0.62
Zr	-11.78	0.194	0.010	15.36	14.97

CoV – coefficient of variation = population standard deviation / mean x100;. CoV of *k* values calculated using all the data points in supplementary Figures S-2 (a), (p), (r) and (t) are given in parenthesis.

$$\beta = \frac{C_O - C_S}{C_L - C_O} = \frac{f_L}{f_S} \tag{3}$$

$$\beta = \sum_{i=1}^{n} \beta_i \tag{4}$$

Eq. 1 captures the phase diagram of the binary alloy system. It can also be seen from Eq. 1 that β is dependent on the nature of solutes, solute concentrations, and solidification conditions. As a result, the precision and accuracy of the *m* and *k* values estimated from Eq. 1 depends not only on the solute-solute interactions but also on the resolution of the binary phase diagram and the values of these parameters, which are not expected to be constant as they might change with alloy composition and temperature [10].

As stated in the paper from which Eq. 3 was derived [8], Eq. 3 implies that the physical meaning of *true* β values is the liquid-to-solid phase fraction. For eutectic systems, $k < 1$, then the difference between β calculated from Eq. 1 and that calculated from Eq. 3 is small and Eq. 1 is a good estimate of values of β. However, for peritectic systems, $k > 1$, such difference is larger and the calculation of β from the ratio of liquid-to-solid fraction (Eq. 3) is more accurate [8]. This accuracy is also dependent on the accuracy of *m* and *k* values.

Additionally, it was derived in their work [8], the growth restriction coefficient ($2/\lambda^2$) which applies to spherical growth during solidification:

$$\frac{2}{\lambda^2} = \frac{1-\alpha}{\alpha(1+\sqrt{\alpha}+\alpha)} \tag{5}$$

A direct relationship between β and the solute supersaturation (α):

$$\alpha = \frac{1}{\beta+1} \tag{6}$$

And, the critical solute concentration C^* for different solute types, calculated by rearranging Eq. 1 at β=0:

$$C^* = \frac{k\Delta T}{m(k-1)} \tag{7}$$

The onset of growth restriction for a specific undercooling is the physical meaning of C^* [8], in that:

if $C_O < C^*$, there is no growth restriction by solute additions (β=0). Solidification becomes partitionless.

if $C_O > C^*$, there is growth restriction of solute, the degree of which increases with increasing C_O as described by Eq. 1.

One outstanding conclusion from their seminal work [8], is that growth velocity is a unique function of *true* β in spite of the nature of solutes, solute concentrations and solidification conditions.

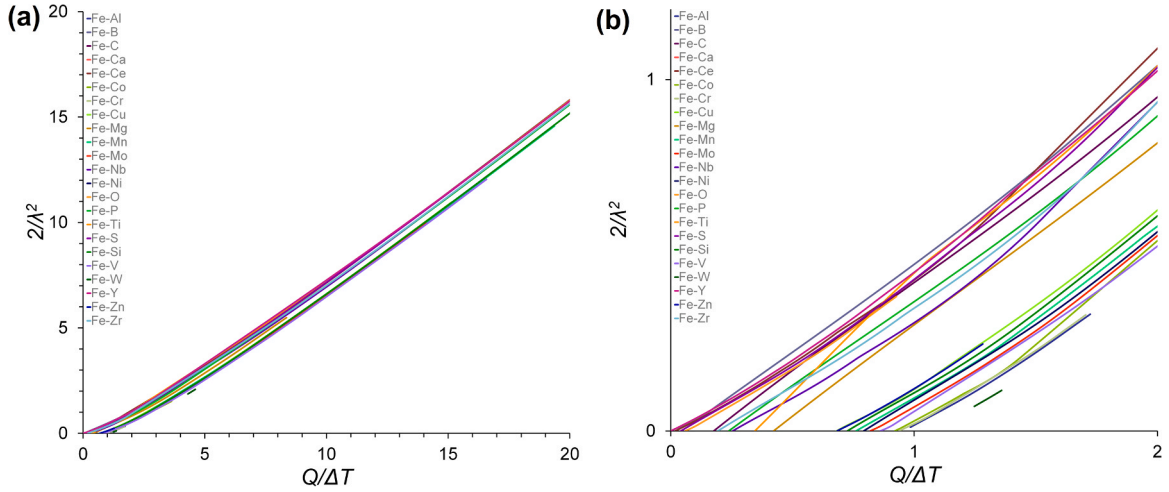

Fig. 1. (**a**) Variation of $2/\lambda^2$ values with the ratio of Q to ΔT at ΔT = 0.5 K for binary ferrous alloys and (**b**) zoom-in region from (a).

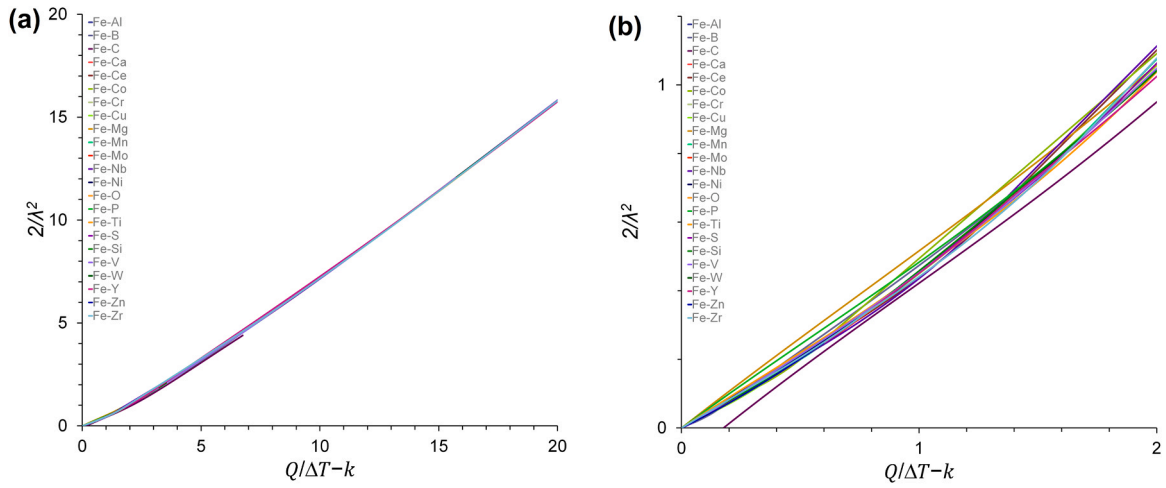

Fig. 2. (**a**) Variation of $2/\lambda^2$ with β values at $\Delta T = 0.5$ K and (**b**) zoom-in region from (a).

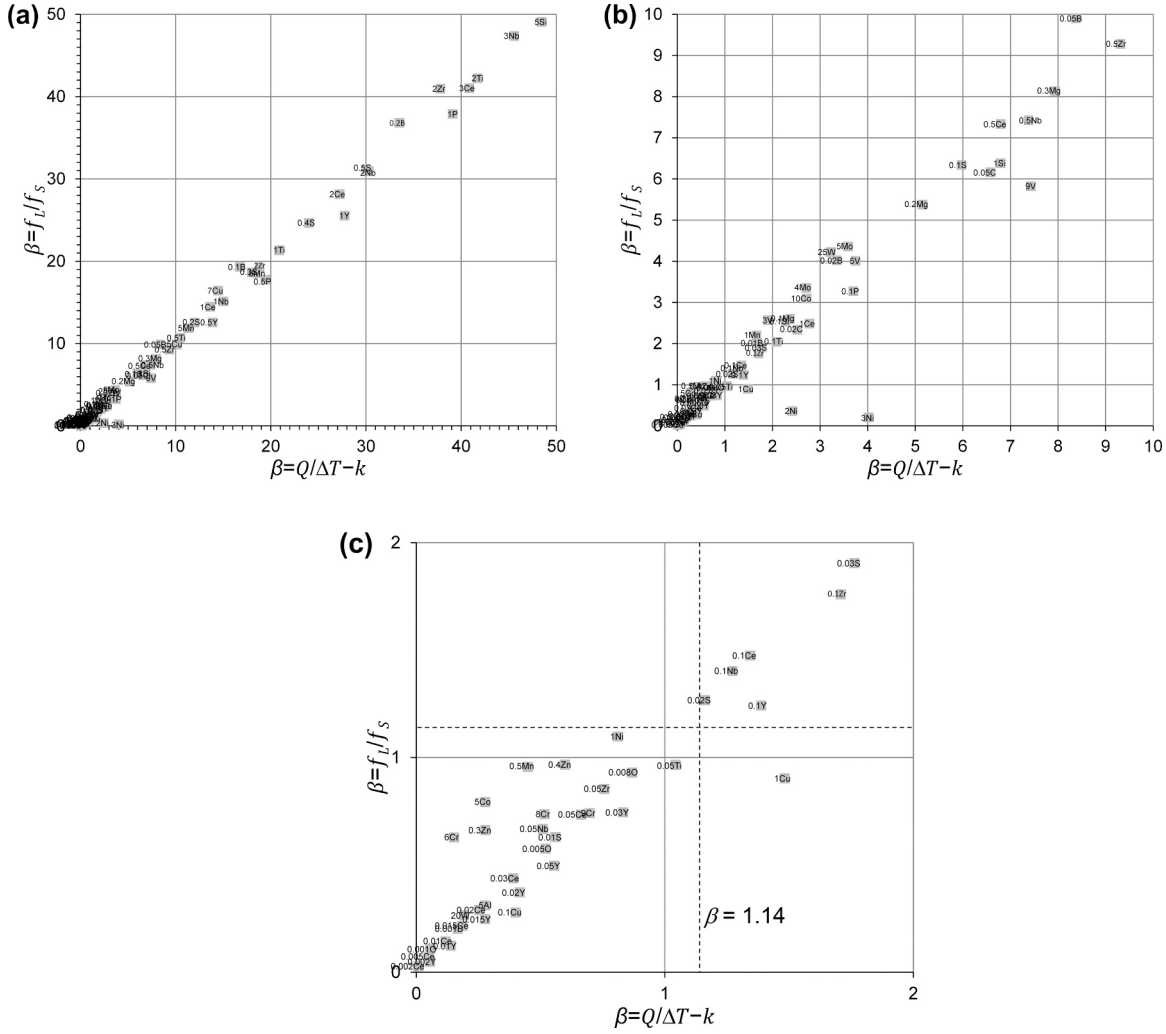

Fig. 3. (**a**) Comparison between the approximated and *true* β values calculated from Eqs. 1 and 3, respectively, for dilute binary ferrous alloys, (**b**) and (**c**) zoom-in regions from (a). The dashed line corresponds to the *true* β of 1.14, which was used as a criterion for CET under a *quasi*-isothermal condition [9] The reader is referred to the web version of this article to zoom-in the alloy compositions given on data point labels.

In a previous study [11], the CALPHAD methodology [10] was successfully used to calculate the heuristic growth restriction parameter (β) for different solutes in Cu-, Al-, Mg- and Ti-based alloys at a constant ΔT value of 0.5 K from the m and k values, at first approximation, as well as from the liquid-to-solid fraction to obtain *true* β values. Data from 65 solutes for Cu-based alloys, 18 solutes for Al-based alloys, 18 solutes for

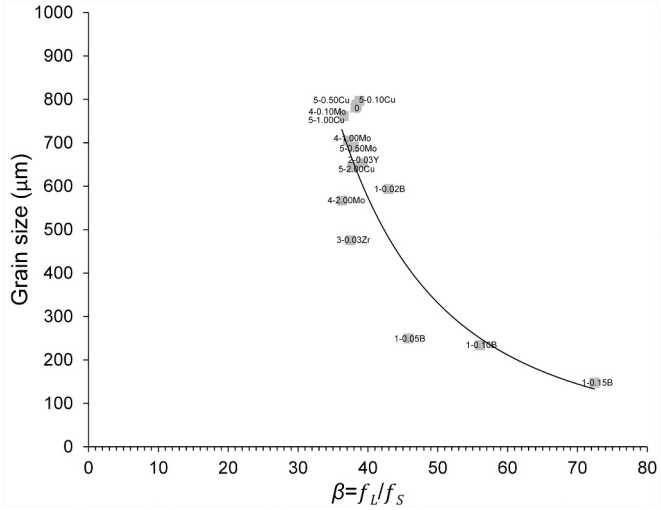

Fig. 4. Variation of equiaxed grain size values from Li et al. [7] with the true β values at ΔT = 0.5 K for different solute additions in dilute ferrous alloys. The 0 point represents the Fe-4Si ferritic alloy system reference without B, Zr, Y, Cu and Mo solute additions. The reader is referred to the web version of this article to zoom-in alloy compositions given on data points labels. The reader is referred to the web version of this article to zoom-in alloy the compositions given on data points labels. The original sample labels from Reference 7 have been kept.

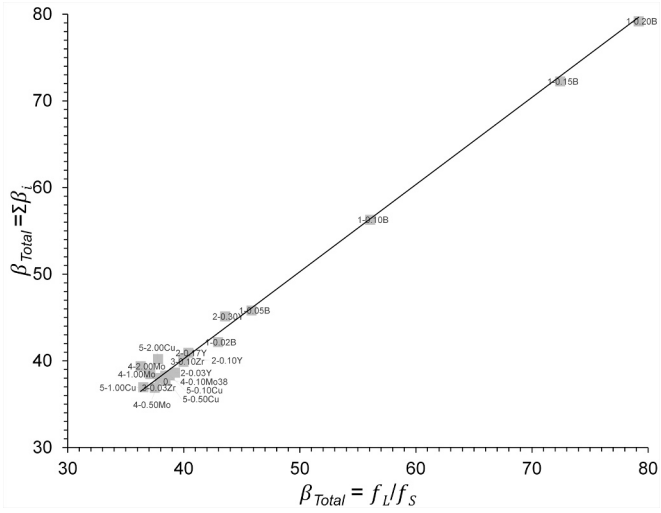

Fig. 5. Comparison between *true* β values calculated using Eq. 3 for the Fe-4Si reference and the multicomponent dilute Fe-4Si-X alloy systems of Reference [7] and those calculated using Eq. 4 for the linear addition of each binary ferrous Fe-X system, β_i. The reader is referred to the web version of this article to zoom-in the alloy compositions given on data points labels. The original sample labels from Reference [7] have been kept.

Mg-based alloys and 26 solutes for Ti-based alloys were input in the calculations. *True* β values for over 500 solidification cooling curves were calculated based on the Gulliver-Scheil cooling conditions for a temperature step of 0.01 K. In another study [11], the heuristic β was calculated in dilute binary ferrous alloys for increased amounts of individual solute additions of Ti, Zr, Nb, V, La, Ce and Y. It was not, however, coupled with experimental data to validate the results.

2. Growth restriction parameter β

Here, the heuristic β has been calculated for dilute binary ferrous alloys. A total of 23 binary Fe-alloy systems have been investigated and over 300 solidification cooling curves have been analyzed. Thermo-Calc Software (version 2023b) [12] has been used for phase analysis and prediction of the Scheil solidification. Grain size values from the aforementioned study [7] were plotted against the corresponding *true* β values for experimental validation in multicomponent dilute ferrous alloy systems.

3. Results and discussion

The Fe-rich regions of the equilibrium phase diagrams for the binary iron alloys of this investigation are plotted in supplementary Fig. S-1. m and k values were determined from supplementary Fig. S-1 (refer to electronic supplementary material), and are listen in Table I. The variation of partition coefficients of solutes with temperature in the L/Fe (bcc) interface for the solidification of dilute binary ferrous alloys are represented in supplementary Fig. S-2. The liquidus slopes in supplementary Fig. S-1 were categorized as linear (C, Ca, Ce, Mg, Mn, Nb, O, P, S, Ti, Y, Zn and Zr), *quasi*-linear (B, Cr, Cu, Mo, Ni and V) and non-linear (Al, Co, Si and W) behavior. The latter were fitted to a set of piecewise linear β from Eq. 1, from which values of m, k and C^* were calculated. Points with filled symbols in supplementary Fig. S-2 were used to obtain mean k values and the corresponding coefficient of variation (CoV) of k. The CoV is defined as the ratio of the population standard deviation to the mean multiplied by 100. Values of C^* at ΔT of 0.5 K were calculated from Eq. 1. Those results are also given in Table I together with weight percentage corresponding to 10 at. percentage and CoV of k.

The CoV values are generally marginally low (<15%), except for additions of Ce as well as additions of S and Ti when calculated using all the data points in supplementary Figs. S-2 (p) and (r). Those results are given in parenthesis in Table I. Similarly, CoV values calculated using all the data points in supplementary Figs. S-2 (a) and (t) are also given in parenthesis in Table I. Therefore, k values at temperatures that cover the solidification range were used to obtain the CoV of k values for Al, S, Ti and W solutes.

The values of the growth restriction coefficient ($2/\lambda^2$) are plotted over the ratio of the *conventional* Q to ΔT and β (Eq. (1)) values for dilute binary iron alloys in Figs. 1 and 2, respectively. From Fig. 1, it is clear that the intercept at the $Q/\Delta T$ axis corresponds to k as highlighted in their work [8]. From Fig. 2, a direct relationship between $2/\lambda^2$ and β values has been found for the dilute Fe-based binary alloys of the present investigation, in agreement with results originally reported by Fan *et al.* [8].

Figs. 3 and 4 compares the calculated β values from Eq. 1, at first approximation, (from the liquidus slope (m) and the equilibrium distribution coefficient (k)), to those calculated using Eq. 3, *true* β (from the liquid-to-solid fraction) for dilute binary ferrous alloy systems. Fig. 3 shows good agreement between the approximated and *true* β values within the scatter of the results. Besides, the dashed lines in Fig. 3(c) at $\beta = 1.14$ refers to the columnar-to-equiaxed transition (CET) criterion under *quasi*-isothermal conditions [9]: i.e. alloys with $\beta < 1.14$ having a columnar grain structure, whereas those with $\beta > 1.14$ having an equiaxed grain structure.

The grain size values in the equiaxed region given in Reference [7] for dilute solute additions are plotted against the calculated *true* β values in Fig. 4. More detailed values are provided in supplementary Table S-I. It can be seen that there is an inverse correlation between grain size and *true* β values. The grain size value for the Fe-4Si ferritic alloy system reference without B, Zr, Y, Cu and Mo solute additions was 780 μm. Y and Zr additions from Reference [7] having an overdose poisoning effect which led to grain coarsening as well as the 1–0.20B steel having a dendritic structure were not included in Fig. 4 as the heuristic β applies on the growth restriction of equiaxed grains. Moreover, *true* β values calculated using Eq. 3 for the multicomponent dilute Fe-4Si-X alloy systems of Reference [7] are compared to those calculated using Eq. 4 for the linear addition of each binary ferrous Fe-X system in Fig. 5, showing excellent agreement between the two approaches.

4. Conclusions

The five most efficient solutes on grain refinement are B, Y, O, S and C, whereas the least efficient are V, Al, Cr, Co and W. Solute efficiency refers to a lesser solute content needed to achieve a certain *true* β value. Y is an uncommon alloying element in steels though. A negative correlation or inverse relationship between equiaxed grain size values and *true* β values has been found in this work in dilute ferrous alloys, in agreement with the results originally reported by Fan et al. [9]. This could suggest the requirement for low S+P impurity levels and the modification of C, Al, Mn and/or Si levels in electrical steels, for example, to control the grain size during solidification for minimizing energy losses in iron, and hence improving the efficiency of electrical motors [1]. Other examples where the modification of C, Al, Mn and/or Si levels could be beneficial to reduce the as-cast grain size are in the case of low-density ferritic steel grades [2].

CRediT authorship contribution statement

Balart María José: Writing – review & editing, Writing – original draft, Validation, Methodology, Investigation, Formal analysis, Conceptualization. **Miani Fabio:** Validation, Supervision, Methodology, Investigation, Formal analysis.

Declaration of Competing Interest

The authors declare that they have no known competing financial interests or personal relationships that could have appeared to influence the work reported in this paper.

Acknowledgement

The support of the EPSRC (UK) is gratefully acknowledged.

Appendix A. Supporting information

Supplementary data associated with this article can be found in the online version at doi:10.1016/j.jalmes.2024.100062.

References

[1] M.F. de Campos, J.C. Teixeira, F.J.G. Landgraf, The optimum grain size for minimizing energy losses in iron, J. Magn. Magn. Mater. 301 (2006) 94–99.
[2] A. Saxena, S.K. Chaudhuri, Correlating the aluminum content with ferrite grain size and core loss in non-oriented electrical steel, ISIJ Int 44 (7) (2004) 1273–1275.
[3] S. Khaple, B.R. Golla, V.V.S. Prasad, A review on the current status of Fe-Al based ferritic lightweight steel, Def. Technol. 26 (2023) 1–22, https://doi.org/10.1016/j.dt.2022.11.019.
[4] R. Rana, C. Lahaye, R.K. Ray, Overview of lightweight ferrous materials: strategies and promises, JOM 66 (9) (2014), https://doi.org/10.1007/s11837-014-1126-5.
[5] T. Yang, C. Lu, G. Velisa, K. Jin, P. Xiu, M.L. Crespillo, Y. Zhang, H. Bei, L. Wang, Effect of alloying elements on defect evolution in Ni-20X binary alloys, Acta Mater. 151 (2018) 159–168.
[6] S.W. Lee, J.H. Ahn, B.M. Moon, D. Kim, S. Oh, Y.J. Kim, H.D. Jung, Preliminary study on FeGd alloys as binary alloys and master alloys for potential spent nuclear fuel (SNF) application, Mater. Des. 194 (2020) 108906, https://doi.org/10.1016/j.matdes.2020.108906.
[7] M. Li, J.M. Li, Q. Zheng, G. Wang, M.X. Zhang, Effect of solutes on grain refinement of as-cast Fe-4Si alloy, Metall. Mater. Trans. A 49A (2018) 2235–2247.
[8] Z. Fan, F. Gao, L. Zhou, S.Z. Lu, A new concept for growth restriction during solidification, Acta Mater. 152 (2018) 248–257.
[9] Z. Fan, F. Gao, Y. Wang, H. Men, L. Zhou, Effect of solutes on grain refinement, Prog. Mater. Sci. 123 (2022) 100809, https://doi.org/10.1016/j.pmatsci.2021.100809.
[10] T.P. Battle, R.D. Pehlke, Equilibrium partition coefficients in iron-based alloys, Metall. Mater. Trans. B 20B (1989) 149–160.
[11] M.J. Balart, F. Gao, J.B. Patel, F. Miani, The Role of Dilute Solute Additions on Growth Restriction in Cu-, Al-, Mg- and Ti-Based Alloys, Metals 12 (2022) 1653, https://doi.org/10.3390/met12101653.
[10] L. Kaufman, H. Bernstein, Computer Calculation of Phase Diagrams, Academic Press, New York, NY, USA, 1970.
[11] Y. Ji, H. Ren, J. Peng, J. Qi, W. Qu, Effect of solutes on refinement of solidification structure in iron-based alloys, Xiyou Jinshu/Chinese, J. Rare Met. 44 (8) (2020) 886–890.
[12] TCFE10-Thermo-Calc Software steels and Fe-alloys database, v10 2023b. Available from: ⟨http://www.thermocalc.com/products-services/databases/thermodynamic⟩.